Atmos. Meas. Tech., 6, 621–635, 2013
www.atmos-meas-tech.net/6/621/2013/
doi:10.5194/amt-6-621-2013

Atmospheric Measurement Techniques
Open Access

Analysis of the potential of one possible instrumental configuration of the next generation of IASI instruments to monitor lower tropospheric ozone

P. Sellitto[1], G. Dufour[1], M. Eremenko[1], J. Cuesta[1], P. Dauphin[1], G. Forêt[1], B. Gaubert[1], M. Beekmann[1], V.-H. Peuch[2], and J.-M. Flaud[1]

[1]Laboratoire Inter-universitaire des Systèmes Atmosphériques (LISA), UMR7583, CNRS, Universités Paris-Est Créteil et Paris Diderot, Rue du Général de Gaulle, 94010 Créteil, France
[2]European Centre for Medium-Range Weather Forecasts (ECMWF), Research Department, Shinfield Park, Reading, Berkshire, RG2 9AX, UK

Correspondence to: P. Sellitto (pasquale.sellitto@lisa.u-pec.fr)

Received: 28 July 2012 – Published in Atmos. Meas. Tech. Discuss.: 21 September 2012
Revised: 12 February 2013 – Accepted: 25 February 2013 – Published: 8 March 2013

Abstract. To evaluate the added value brought by the next generation of IASI (Infrared Atmospheric Sounder Interferometer) instruments to monitor lower tropospheric (LT) ozone, we developed a pseudo-observation simulator, including a direct simulator of thermal infrared spectra and a full inversion scheme to retrieve ozone concentration profiles. We based our simulations on the instrumental configuration of IASI and of an IASI-like instrument, with a factor 2 improvement in terms of spectral resolution and radiometric noise. This scenario, that will be referred to as IASI/2, is one possible configuration of the IASI-NG (New Generation) instrument (the configuration called IASI-NG/IRS2) currently designed by CNES (Centre National d'Études Spatiales). IASI-NG is expected to be launched in the 2020 timeframe as part of the EPS-SG (EUMETSAT Polar System-Second Generation, formerly post-EPS) mission. We produced one month (August 2009) of tropospheric ozone pseudo-observations based on these two instrumental configurations. We compared the pseudo-observations and we found a clear improvement of LT ozone (up to 6 km altitude) pseudo-observations quality for IASI/2. The estimated total error is expected to be more than 35 % smaller at 5 km, and 20 % smaller for the LT ozone column. The total error on the LT ozone column is, on average, lower than 10 % for IASI/2. IASI/2 is expected to have a significantly better vertical sensitivity (monthly average degrees of freedom surface–6 km of 0.70) and to be sensitive at lower altitudes (more than 0.5 km lower than IASI, reaching nearly 3 km). Vertical ozone layers of 4 to 5 km thickness are expected to be resolved by IASI/2, while IASI has a vertical resolution of 6–8 km. According to our analyses, IASI/2 is expected to have the possibility of effectively separate lower from upper tropospheric ozone information even for low sensitivity scenarios. In addition, IASI/2 is expected to be able to better monitor LT ozone patterns at local spatial scale and to monitor abrupt temporal evolutions occurring at timescales of a few days, thus bringing an expected added value with respect to IASI for the monitoring of air quality.

1 Introduction

Air quality (AQ) pertains to the characterization of the atmospheric composition at the lowest altitude levels, in terms of both trace gas concentrations and aerosol burden and composition. It is increasingly evident how pollution in the lower troposphere (LT) and a poor AQ have an onerous impact on human health and environment, and then on society. An average reduction of up to several months in life expectancy in European urban areas, due to exposure to higher levels of pollutants like ozone or particulate matter, has been hypothesized (Amann et al., 2005). One of the most important parameters to characterize AQ is the ozone concentration in the LT (WMO, 2002). Tropospheric ozone is a secondary air

pollutant (in the lower troposphere) and also acts as a greenhouse gas (in the upper troposphere) (Shindell et al., 2009). Ozone levels in the troposphere are mainly determined by two distinct phenomena: stratosphere/troposphere exchanges (STE) and photochemical production partially linked to human emitted primary pollutants (WMO, 2002). In the last decades, this latter source of tropospheric ozone has started to be considered as more important than STE (WMO, 2002), raising the interest of the human impact on AQ (Crutzen and Stoermer, 2000). Some recent studies have shown that the ozone levels in troposphere may have been increased up to 50 % by human activity from the pre-industrial age, and present projections on future emission rates may lead to a further increase of 40 % (for the worst case scenario) by 2100, the largest increase occurring at northern mid- to high-latitudes (Horowitz, 2006). In spite of the clear reduction of ozone precursors' concentrations (Monks et al., 2009) over the US and Europe, mean ozone concentrations in the troposphere, and even at the surface, do not show a corresponding clear decreasing trend (Wilson et al., 2012). Moreover, in the global warming framework, events of severe photochemical pollution, with possible significant enhancements of ozone concentrations at surface and in the LT, are likely to become more and more frequent (Schär and Jendritzky, 2004; Vautard et al., 2005; Ran et al., 2009). In addition, the lifetime of ozone precursors and ozone itself can be very variable (from days to months). Ozone concentrations in the LT, correspondingly, can be very variable both in time and in space. In this complex framework, it is very important to monitor the levels and evolution of LT ozone at those various space–time scales. Indeed, both local production of ozone (Ran et al., 2009) and transport at small to continental (and sometimes intercontinental) scales (Lin et al., 2012) concur to determine local LT ozone levels.

Monitoring AQ from space is a topical issue in modern geosciences, see, e.g. the review done by Martin (2008). In the last few years, the use of satellites for the observation of relevant AQ parameters, like LT ozone concentration or other trace gases associated with air pollution, has undergone significant advances with new and exciting perspectives in atmospheric pollution monitoring. Satellite instruments flying in low Earth orbit (LEO) and observing the Earth with nadir geometry have proved to be able to retrieve the tropospheric ozone information, both exploiting the backscattered ultraviolet (UV) radiances, e.g. (Fishman and Larsen, 1987; Munro et al., 1998; Ziemke et al., 2003; Liu et al., 2005; Schoeberl et al., 2007; Liu et al., 2010; Sellitto et al., 2011), the synergy ultraviolet/visible (UV/VIS) (Sellitto et al., 2012a,b), and the thermal infrared (TIR) emitted spectra, e.g. (Worden et al., 2007a; Eremenko et al., 2008). Some simulation experiments of combining the TIR and the UV/VIS have also been recently done (Worden et al., 2007b; Landgraf and Hasekamp, 2007; Natraj et al., 2011), as well as some first attempts with real measurements (Fu et al., 2012; Cuesta et al., 2013). TIR measurements, in particular those obtained by the Infrared Atmospheric Sounding Interferometer (IASI), have been shown to have the capability of further distinguish the LT ozone information (up to 6 km altitude) in the presence of higher thermal contrasts, i.e. for high sensitivity scenarios (Dufour et al., 2010). In a comparative study with ozonesondes reference data involving 3 different scientific ozone products derived from IASI observations, Dufour et al. (2012) found that LT ozone columns are derived with a total error ranging from 15 to 20 % and with 0.3 to 0.6 degrees of freedom (DOF); these results evidenced that it is, in general, not always possible to derive a reliable and independent information on LT ozone from IASI. Notice that one of the three inversion schemes used in the mentioned paper, hereafter mentioned as the *LISA algorithm*, is the inversion scheme used in the present work.

New generation observing systems are envisaged to improve the capability to monitor tropospheric composition in detail, including AQ. In this context, one of the existing projects is IASI-NG (Infrared Atmospheric Sounding Interferometer-New Generation) (Crevoisier et al., 2012; Clerbaux and Crevoisier, 2013). IASI-NG is expected to be launched in the 2020 time frame as part of the EUMETSAT Polar System-Second Generation (EPS-SG) programme (formerly called post-EPS programme). The instrument will be a Fourier transform spectrometer. Its scientific objectives are to assure the continuity of the IASI mission for the needs of numerical weather prediction, atmospheric composition and climate studies, to improve the vertical resolution and precision of the retrieved variables, and to enable the detection of new species. IASI-NG has recently accomplished the phase A stage (Crevoisier et al., 2012) and follows heritage of IASI. During this design activity, different possible configurations of IASI-NG have been proposed. The one described in the following lines is called IASI-NG/IRS2 by Crevoisier et al. (2012). This configuration is hereafter referred to as IASI/2. The IASI/2 concept has a similar horizontal resolution as IASI, with a pixel size of 12 km diameter at the nadir. The spectral sampling interval (SSI), spectral resolution and radiometric noise are improved by a factor of 2. The SSI and spectral resolution for this configuration are then expected to have values of $0.125\,\mathrm{cm}^{-1}$, $0.25\,\mathrm{cm}^{-1}$, and a radiometric noise, in terms of the noise equivalent spectral radiance (NESR), of $10\,\mathrm{nW/(cm^2\,sr\,cm^{-1})}$, in the spectral band relevant for ozone retrievals (around 10 µm). A factor 2 improvement of the spectral and noise characterization with respect to IASI is expected to bring a clear added value in the observation capabilities into the LT, both in terms of systematic and random errors, and of vertical resolution.

In this paper, we present a study aimed at comparing the performances of IASI/2 and IASI for the monitoring of LT ozone. We will quantify the improvement of IASI/2 with respect to IASI for the observation of phenomena developing at time–space scales relevant for AQ. The main question that we want to address is to evaluate if IASI/2 would be a clear step forward toward a better monitoring of AQ,

in terms of both local and short-term LT ozone evolutions. Another objective is to determine if its added value is limited to a better characterization of continental scale phenomena. To this end, spatial and temporal features are both investigated at those different scales. We based our analysis on the so-called *pseudo-observations* generated by a newly developed pseudo-observation simulator. Using reference trace gases and meteorological fields, the so-called *pseudo-reality*, for a given period over Europe, the simulator calculates the TIR spectra including noise and then inverts them to retrieve ozone concentration profiles with a full inversion scheme. The selected study period is August 2009. This period is characterized by some interesting pollution events, like a tropospheric ozone plume developing in the period 19–21 August, with ozone-rich air masses extending from southern France to the Scandinavian Peninsula. The set-up of our pseudo-observations simulator, including the retrieval scheme, is described in Sects. 2.1 and 2.2. The error and vertical resolution characterization of the IASI and IASI/2 pseudo-observations is given in Sects. 3.1 and 3.2. We carried out a general statistical characterization of the pseudo-observations for the two observing systems and this is discussed in Sect. 4.1. We then studied the added values brought by IASI/2 in monitoring both LT ozone distribution at continental and regional scales (Sect. 4.2), and at a local scale (Sect. 4.3). This latter spatial scale is the most important for AQ. Finally, in Sect. 5 we give conclusions.

2 IASI and IASI/2 pseudo-observations

2.1 Pseudo-observations simulator

The pseudo-reality, in terms of both the meteorological variables and the trace gases concentrations, including the target ozone fields, is produced by means of the MOCAGE (MOdèle de Chimie Atmosphérique à Grande Echelle) chemistry and transport model (CTM). MOCAGE simulates the physical and chemical processes affecting gases and aerosols in both the troposphere and the stratosphere, e.g. Dufour et al. (2005). MOCAGE uses 47 hybrid vertical levels, from surface to about 35 km, with a fine vertical grid, from about 200 m into the lower troposphere to about 1 km into the stratosphere. The outputs of MOCAGE have been resampled to the smaller vertical resolution required by the subsequent radiative transfer calculation, 1 km into the troposphere and lower stratosphere, and 2 to 5 km at higher altitudes. Topography data have been taken from GTOPO30 (Global 30 Arc Second Elevation Data Set) digital elevation model (http://www1.gsi.go.jp/geowww/globalmap-gsi/gtopo30/gtopo30.html). Trace gas concentrations, pressure, temperature and specific humidity vertical profiles at the mentioned vertical resolutions are obtained and used as inputs for the radiative transfer (RT) calculations. For the present work, the presence of clouds has not been considered.

The Karlsruhe Optimized and Precise Radiative transfer Algorithm (KOPRA) radiative transfer model (RTM) (Stiller et al., 2002) is used to simulate the radiation spectra viewed by the selected instruments. This model, formerly developed to simulate MIPAS (MIchelson Interferometer Passive Atmospheric Sounding) limb measurements, has been adapted to the nadir geometry (Eremenko et al., 2008). The two instruments, IASI and IASI/2, are defined by their technical specifications. The observation geometry has been taken from real IASI measurements at the corresponding date of each simulation. An instantaneous field-of-view set-up of a 2×2 horizontal array of pixels of 12 km diameter each and spaced by 25 km at nadir has been accordingly considered. We have made the hypothesis of the same observation geometry for IASI/2. IASI overpasses Europe twice a day, at about 09:00–10:00 UTC and 21:00–22:00 UTC. We simulated both overpasses, hereafter referred to as AM and PM overpasses. The nadir spectra, in the region of interest (latitude: 35° N–70° N, longitude: 15° W–35° E), are then about 18 000 for each overpass, so more than 1 million for the whole study period (August 2009). The instrumental spectral sampling and radiometric noise have been modelled by the SSI and the NESR. The SSI of IASI is $0.25\,\mathrm{cm}^{-1}$, corresponding to a $0.50\,\mathrm{cm}^{-1}$ apodized spectral resolution (optical path difference of 2 cm), while the NESR is $20.0\,\mathrm{nW/(cm^2\,sr\,cm^{-1})}$ (Clerbaux et al., 2009). IASI/2 improves by a factor of 2 in both spectral resolution and radiometric noise (Crevoisier et al., 2012). The SSI and NESR for IASI/2 are, accordingly, $0.125\,\mathrm{cm}^{-1}$ ($0.25\,\mathrm{cm}^{-1}$ apodized spectral resolution, 4 cm optical path difference) and $10.0\,\mathrm{nW/(cm^2\,sr\,cm^{-1})}$.

2.2 Inversion algorithm

The simulated spectra are inverted by means of the KOPRAfit module (Hoepfner et al., 2001) embedding a dedicated algorithm based on a constrained least squares fit method to obtain pseudo-observations of ozone profiles. The pseudo-observations can be, then, finally compared with the pseudo-reality to evaluate possibilities and limits of the selected observing system. The KOPRAfit also provides the averaging kernels (AKs), that can be used to derive the information on the vertical sensitivity of the different configurations over several conditions defined, e.g. by the meteorology and surface characteristics.

The inversion algorithm used to derive the pseudo-observations, referred to as LISA algorithm (Eremenko et al., 2008), is an altitude-dependent Tikhonov–Phillips regularization method embedded into the KOPRAfit retrieval module using the KOPRA RTM. Altitude dependent Tikhonov–Phillips regularization methods for satellite nadir measurements were introduced by Kulawik et al. (2006); the method is here optimized for LT (surface–6 km) ozone observations using IASI measurements (Eremenko et al., 2008). The

constraint matrix is a combination of the identity matrix, and the first and the second derivative operator, with coefficients depending on the altitude. The constraint matrix and parameters of the LISA algorithm are optimized to maximize the degrees of freedom (DOF) and minimize the error in the LT while retaining a sufficient accuracy in the upper troposphere and in the stratosphere. Dufour et al. (2012) evaluated the performances of ozone profiles obtained by means of the LISA algorithm with a validation exercise using ozonesondes measurements and verified the enhanced performances in the LT, if compared to other scientific retrieval schemes. In their validation, the mean DOF of the LISA algorithm is in the range 0.4–0.6 and the estimated error in LT ozone column is about 12.5 %, at mid-latitudes. The ozone a priori profiles used in the present work are derived from McPeters climatology (McPeters et al., 2007). To avoid numerical instability and aberrant oscillations in the retrieved profiles, we used a different a priori depending on tropopause height derived from the pseudo-reality. We consider a tropopause higher than 14 km as a proxy for tropical air masses and then we used a tropical a priori (yearly climatological profile 20–30° N) in those cases. We used a mid-latitude a priori (summer climatological profile 30–60° N) in the other cases. The use of two different a priori, in particular mid-latitude and tropical climatological profiles, has been already successfully exploited for the LISA algorithm (Dufour et al., 2010). The LISA algorithm operates at seven spectral microwindows, in the region of 975–1100 cm^{-1}, to avoid carbon dioxide and water vapour impact on ozone retrievals. For more details, please refer to the comprehensive description of the LISA algorithm of Eremenko et al. (2008); Dufour et al. (2010).

3 Characterization of the pseudo-observations

3.1 Error estimation for IASI and IASI/2 tropospheric ozone retrievals

In this section, we provide a comparative analysis of the error budget estimated for IASI and IASI/2 pseudo-observations.

According to Rodgers (1990), if the inversion occurs in an incrementally linear regime, the total error budget of a constrained least squares fit method can be separated into three main components: (a) measurement noise (random) error, (b) smoothing error due to the limited vertical resolution of the observing system, and (c) systematic error. Equation (1) describes analytically these three error components, the smoothing, the measurement noise and the systematic error, respectively. **A** is the averaging kernel matrix, that is extensively analysed and discussed in Sect. 3.2, **G** is the gain matrix, $\mathbf{K}_{syst}$ is the Jacobian matrix for the systematic errors and **I** is the identity matrix. The covariance matrices for the total error, the a priori ozone variability, the measurement noise and the systematic error are here indicated as $\mathbf{S}_e$, $\mathbf{S}_a$, $\mathbf{S}_m$ and $\mathbf{S}_{sys}$. $\mathbf{S}_a$ is obtained with the climatology of McPeters et al. (2007) for mid-latitude summer conditions, as done by Eremenko et al. (2008), where the smoothing error is evaluated on a 1-km grid.

$$\mathbf{S}_e = (\mathbf{I}-\mathbf{A})\,\mathbf{S}_a\,(\mathbf{I}-\mathbf{A})^T + \mathbf{G}\mathbf{S}_m\mathbf{G}^T + \mathbf{G}\mathbf{K}_{syst}\mathbf{S}_{syst}\left(\mathbf{G}\mathbf{K}_{syst}\right)^T \quad (1)$$

This formulation, valid for an optimal estimation method (Rodgers, 2000), can be applied also to general regularization methods, provided the symmetry of the a priori covariance and the regularization matrix as the constraints of the least square minimisation (Steck and von Clarmann, 2000).

Figure 1a and b show the mean measurement, smoothing and total error (in absolute, Fig. 1a, and percent units, Fig. 1b), for IASI and IASI/2 pseudo-observations, averaged over all pixels of the day 20 August 2009, for the AM overpass. The results for the PM overpass are very similar (not shown here). The mid-latitude a priori and pseudo-reality variability are also shown as a reference. The first one is given by the diagonal elements of the mid-latitude a priori covariance. The errors for this day are quite representative of the other days and of individual pixels. The dominant error component is the smoothing error. It has values of about 25 % at the surface for the two instruments, 15–20 % for IASI/2 and 20–25 % for IASI in the interval 2–6 km, and 20–25 % for IASI/2 and 20–30 % for IASI in the interval 7–12 km. For the measurement noise error, we found typical values of 3–4 % at the surface for the two instruments, 3–7 % for IASI/2 and 6–9 % for IASI in the interval 2–6 km, and 3–12 % for IASI/2 and 7–11 % for IASI in the interval 7–12 km. Correspondingly, total error typical values were about 30 % (10.2 ppb) at the surface for the two instruments, 22–30 % (8.3–9.9 ppb) for IASI/2 and 30–35 % (10.3–15.5 ppb) for IASI in the interval 2–6 km, and 24–40 % (10.4–44.6 ppb) for IASI/2 and 30–40 % (12.2–50.2 ppb) for IASI in the interval 7–12 km. Figure 1c summarizes these results as a percent improvement of IASI/2 error over IASI error, defined as the percent difference of the absolute measurement, smoothing and total errors of IASI/2 and IASI. The improvement is particularly significant for the smoothing component in the range 1–5 km and for the measurement noise component in the range 3–7 km. The improvement of the total error reaches values higher than 35 % at 5 km. The errors on the tropospheric ozone column (TOC) for IASI and IASI/2 are: 3.81 DU (10.51 %) and 3.12 DU (8.41 %), for the surface–12 km TOC, and 2.49 DU (14.01 %) and 2.06 DU (10.71 %), for the surface–6 km TOC. The error values for the IASI pseudo-observations are generally consistent with those for IASI real measurements (Eremenko et al., 2008; Dufour et al., 2012). It must be considered that in our estimation and in the paper by Dufour et al. (2012) only measurement noise and smoothing error are considered, while Eremenko et al. (2008) considered also temperature profile errors and other systematic error sources. These components

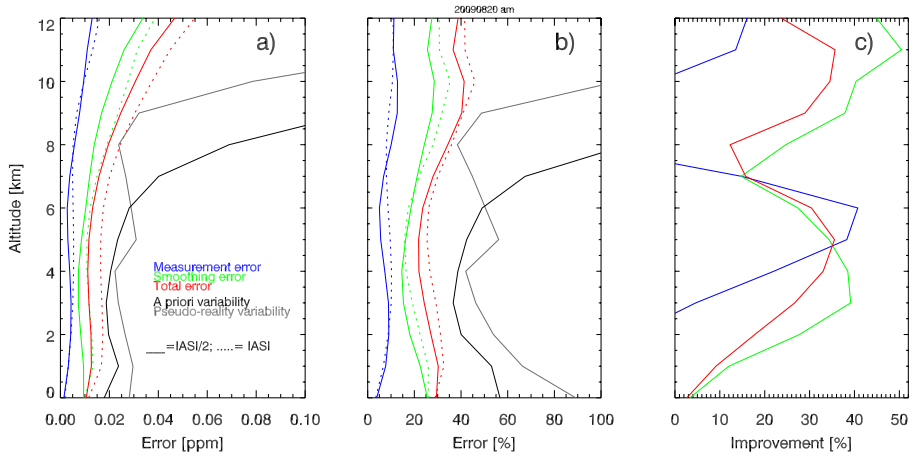

Fig. 1. Mean values for 20 August 2009, AM overpasses, of the estimated measurement (blue), smoothing (green) and total error (red), for IASI (dotted lines) and IASI/2 (solid lines): **(a)** absolute errors, **(b)** percent errors, **(c)** percent improvement of IASI/2 over IASI. A priori (black line) and pseudo-reality variability (grey line) are also shown.

may explain the small difference between our IASI pseudo-observations and IASI real measurements error analysis described by Eremenko et al. (2008). Indeed, error components other than smoothing and measurement noise usually contribute a few percent (Boynard et al., 2009). From the comparison of the two sets of pseudo-observations, we found that errors on the surface–6 km TOC, taken as representative of the LT ozone, are nearly 20 % smaller for IASI/2.

3.2 Averaging kernels shape and vertical sensitivity to ozone

In the following, we discuss and compare some important quantities to characterize the pseudo-observation of IASI and IASI/2, with emphasis on the vertical resolution. To do so, we analyse the AKs shape and some derived quantities.

The **AK** matrix has already been introduced in Sect. 3.1 for its role in determining the smoothing error component. The **AK** matrix represents the sensitivity of the retrievals to the true profile. Each **AK** matrix row shows the fractional height-resolved source of information for the retrieval at the selected altitude. For higher values, a greater fraction of information is taken from the observed spectrum, the remaining fraction coming from the a priori. In Fig. 2, we show the **AK** rows for nominal altitudes from surface to 12 km, for the two instruments, calculated as means over all pixels in August 2009 with thermal contrast lying into a chosen interval. We show the average AKs for pixels with thermal contrast in the interval [+8.0, +9.0] K, as representative of high sensitivity scenarios, and [−9.0, −8.0] K as representative of low sensitivity scenarios. The greatest added value of IASI/2 emerges for the small sensitivity scenarios. There, IASI/2 pseudo-observations have a significantly better vertical sensitivity, represented by narrow functions peaking at lower altitudes. In general, we found significantly better performances of the IASI/2 in presence of small/negative thermal contrasts.

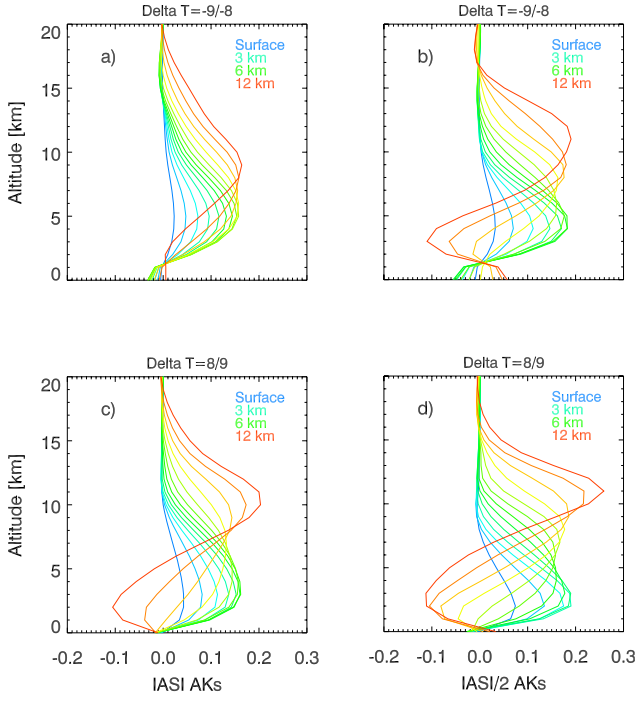

Fig. 2. Averaging kernel functions from surface (sky blue) to 12 km (red) for IASI: **(a)** low sensitivity scenario, and **(c)** high sensitivity scenario, and IASI/2: **(b)** low sensitivity scenario, and **(d)** high sensitivity scenario. The functions are means over the whole period of study (August 2009).

In Fig. 3, we also show the integral AKs calculated for the ozone columns surface–6 km, 7–12 km and surface–12 km, as representative of the lower, the upper and the whole troposphere. What we found is that the integral AKs of IASI/2 for the lower and upper troposphere are well separated also for small sensitivity scenarios (see Fig. 3b), thus confirming the previous findings. For IASI, on the contrary, the integral

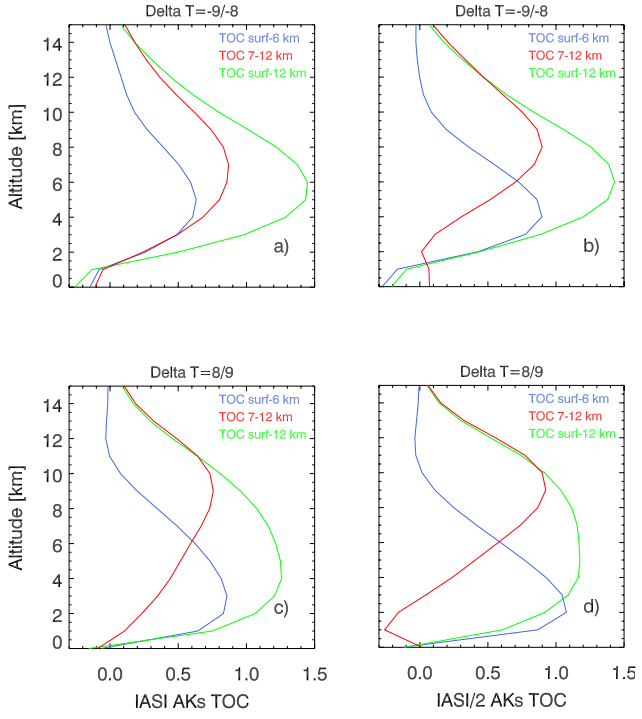

Fig. 3. Integral averaging kernel functions for the TOCs surface–6 km (blue), 7–12 km (red) and surface–12 km (green) for IASI: **(a)** low sensitivity scenario, and **(c)** high sensitivity scenario, and IASI/2: **(b)** low sensitivity scenario, and **(d)** high sensitivity scenario. The functions are means over the whole period of study (August 2009).

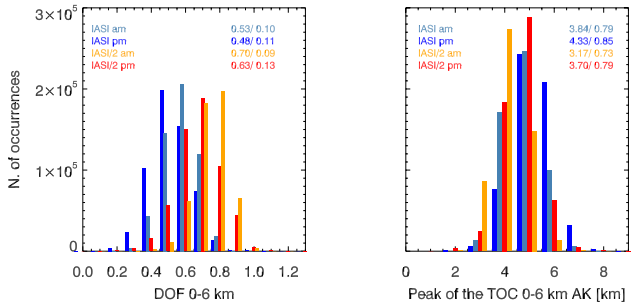

Fig. 4. Histogram of the DOF surface–6 km (left) and of the altitudes of the maximum of the integral AK for the surface–6 km TOC (right), for AM and PM overpasses, for IASI (sky blue and blue) and IASI/2 (orange and red). Mean values and standard deviations are also reported in the upper right corners (mean/std). The data cover the whole period of study (August 2009).

AKs surface–6 km and 7–12 km are partially overlapped in low sensitivity scenarios (see Fig. 3a), thus indicating that our IASI pseudo-observations have not the potential to single out the LT information component in those cases. This result is coherent with several studies dealing with tropospheric ozone retrievals from IASI, e.g. Dufour et al. (2010). On the other hand, the separation of lower to upper tropospheric ozone information is more possible with IASI/2 over several scenarios, both with higher and lower/negative thermal contrast.

Other two valuable diagnostic parameters to study the vertical sensitivity of a retrieval are the DOF and the altitude of the maximum of the AKs. DOF is a quantity that indicates the number of independent pieces of information that can be determined from a measurement. It is linked to the **AK** matrix by means of the following relationship (Rodgers, 2000)

$$\mathrm{DOF} = tr(\mathbf{A}). \quad (2)$$

DOF for ozone partial columns are obtained from the **AK** matrix by calculating the trace up to the top height of the column. It is straightforward how the total DOF or the DOF for the partial columns can be seen as one scalar quantity, which describes the more complex **AK** matrix quantity in terms of the vertical sensitivity of the retrieval. This parameter is complemented by the altitude of the maximum of the AK of a selected altitude or column. In the following, we will concentrate on the altitude of the maximum of the integral AK of the surface–6 km TOC, which represents the altitude of maximum sensitivity of the observations of the surface–6 km TOC. Figure 4 shows the histogram of DOF surface–6 km and altitude of maximum sensitivity for all the observations in August 2009. Results for AM and PM overpasses are reported separately. DOFs from surface–6 km are more than 30 % higher for IASI/2 reaching a mean value as high as 0.70 for the AM overpass, while IASI has a mean value of 0.53. The altitude of the maximum sensitivity of IASI/2 for the surface–6 km TOC is more than 0.5 km lower than for IASI, reaching a mean value of nearly 3.0 km for the AM overpass. The PM overpass is characterized by a significantly lower vertical sensitivity for both instruments. This can be related to the smaller thermal contrasts that characterize, on average, the PM overpasses. The mean values of the DOF surface–6 km, at PM, are about 10 % smaller than for AM overpasses, in particular 0.63 and 0.48 for IASI/2 and IASI, respectively. The maximum sensitivity is found more than 0.5 km higher than for AM overpasses, on average, and in particular at 3.7 and 4.3 km for the two instruments. Nevertheless, it should be noticed that the mean DOF at PM overpass for IASI/2 is higher than the mean DOF for IASI at AM overpass. Moreover, the mean maximum sensitivity altitude is lower for the PM overpass of IASI/2 than for the AM overpass of IASI. The vertical sensitivity in the LT of IASI/2 at PM is then comparable to that of IASI at AM.

The analyses of this and the previous sections clearly show the improved precision and vertical sensitivity in the LT of IASI/2. In the next sections, we analyse how this potential is expected to impact on the observation capabilities in the LT, in particular for the tropospheric ozone monitoring at both continental/regional and local scales.

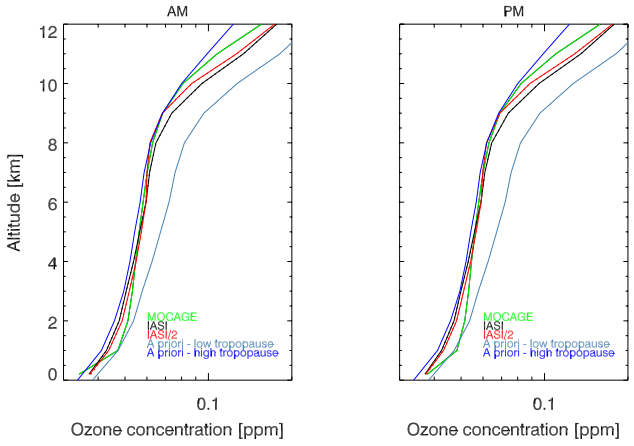

Fig. 5. Mean ozone profiles for August 2009, for MOCAGE pseudo-reality (green line), IASI (black line) and IASI/2 pseudo-observations (red line), low tropopause/mid-latitude (sky blue line) and high tropopause/tropical a priori (blue line); AM (left), PM (right)

4 LT ozone distributions retrieved by IASI and IASI/2

4.1 Global analysis

In the present section, we give a global characterization of the pseudo-observations. To this end, we have performed a general statistical analysis of IASI and IASI/2 tropospheric ozone profile and surface–6 km TOC pseudo-observations, by comparing them to the reference MOCAGE pseudo-reality, based on several statistical parameters. Please note that the pseudo-reality used in this analysis is not convolved with the AKs.

Figure 5 shows the monthly average ozone profiles in the troposphere from pseudo-reality, and IASI and IASI/2 pseudo-observations for AM and PM overpasses. As a further reference, the two a priori profiles are also shown on the plots. It is clear that both IASI and IASI/2 pseudo-observations underestimate the pseudo-reality in the interval 1–4 km and overestimate the pseudo-reality in the range 9–12 km. This effect is more marked for IASI. AM and PM overpasses behave in a quite similar manner. Please note how the low tropopause/mid-latitude and the high tropopause/tropical a priori respectively overestimate and underestimate the mean pseudo-reality ozone profile. This effect has an impact on the pseudo-observations and it will be recalled later during the interpretation of their behaviour. Figure 6 shows the percent bias, the percent RMSE and the linear correlation (Pearson) coefficient profiles for IASI and IASI/2, with respect to pseudo-reality, for AM and PM overpasses. In Table 1, the same parameters are reported as vertical averages in the intervals 0–3 km, 0–6 km, 0–12 km and 7–12 km. For both instruments, the bias is negative from 0 to 4 km, tends to be very small from 4 to 8 km, and it is positive at higher altitudes, reaching values as high as 15 %

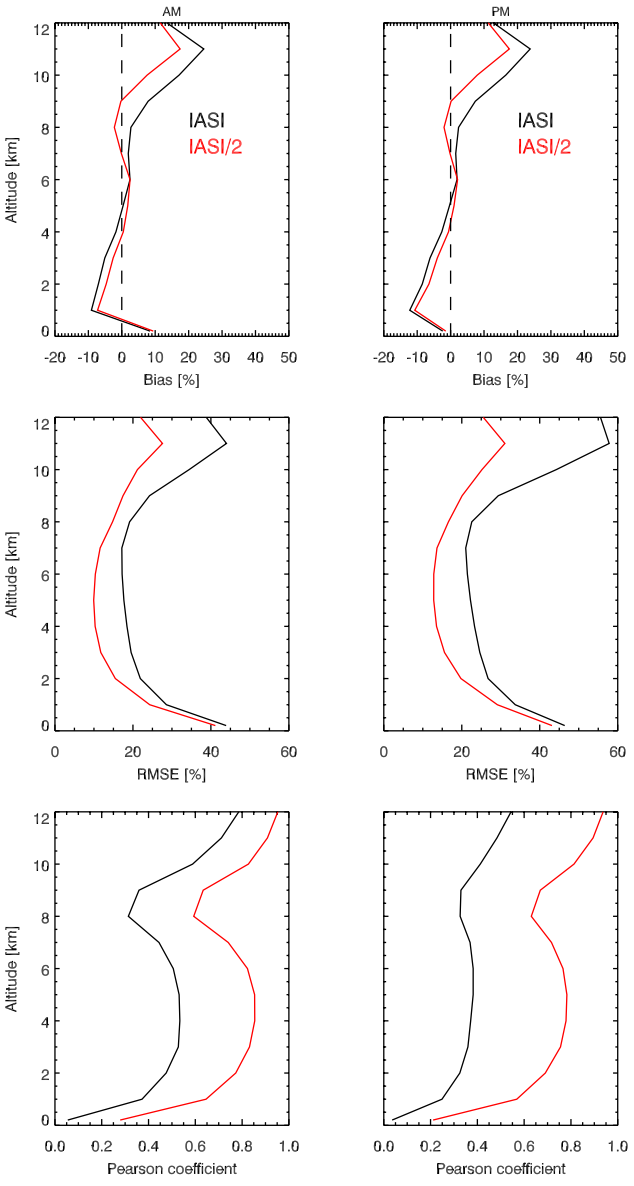

Fig. 6. Mean percent bias (top), percent RMSE (middle), Pearson coefficient (bottom) vertical profiles, AM (left) and PM (right), for IASI (black lines) and IASI/2 pseudo-observations (red lines). All quantities are calculated with the ensemble of simulations for August 2009.

for IASI/2 and 25 % for IASI. The negative bias of the AM overpass for IASI of about the 3 % in the range 0–3 km, as well as the positive bias of about the 11.5 % in the range 7–12 km are reduced by about 50 % with IASI/2 (see Table 1). Also for the PM overpass, the biases are strongly reduced by IASI/2. The underestimation at the lowest levels may be due to the small sensitivity and the different impact of the a priori profiles. The high tropopause/tropical a priori is strongly negatively biased in the range surface–3 km (see Fig. 5) and may certainly transmit this negative bias to the pseudo-observations. The AKs, indeed, are generally very

small at those altitudes and a strong contribution of the a priori is expected on the pseudo-observations. On the contrary, the low tropopause/mid-latitude a priori has similar values with respect to pseudo-reality in that range. The net effect on the overall data set is likely to be a negative bias. The negative bias is less important for IASI/2 because this latter instrument has a better sensitivity at the lowest altitudes and then a smaller contribution of the a priori. As for the overestimations in the range 8–12 km, this is coherent with the validation results of Dufour et al. (2012). A systematic overestimation (10 to 25 %) of ozone in the upper troposphere–lower stratosphere by the three products based on real IASI data validated versus ozonesondes data is shown by Dufour et al. (2012). Overestimations of the same order of magnitude are also found for our IASI pseudo-observations. As for the RMSE, the lowest values are in the range 2–8 km (where the information provided by IASI and IASI/2 spectra contribute the most), reaching values as small as 10 % for IASI/2 and 20 % for IASI, for the AM overpass, and 12 % and 23 %, for the PM overpass. The Pearson correlation coefficient over the whole data set has the more significant differences between IASI and IASI/2. The vertical profile has two maxima, one at about 4 km and one at 12 km. At those maxima, typical values for IASI are 0.50–0.75 while IASI/2 can reach values of 0.90–0.95, for the AM overpass. In addition, while IASI/2 performances for the AM and PM overpasses are quite similar, the IASI pseudo-observations performances at PM show a significant degradation, especially in the range 0–6 km, where a vertically averaged value of 0.30 is found (see Table 1). This behaviour can be easily associated with the results of Sect. 3.2, and in particular of Fig. 3. In fact, it has been shown that the performances of IASI are particularly weak at unfavourable conditions, i.e. in presence of small/negative thermal contrasts. IASI/2, on the contrary, performs quite well also over low sensitivity scenarios. During the PM overpass, small/negative thermal contrasts are significantly more frequent and then the added value brought by IASI/2 is more critical. In general, biases and RMSEs of the profiles are systematically smaller and correlations are systematically higher for IASI/2, reaching an improvement of 26 % (RMSE) and 67 % (correlation) with respect to IASI in the range surface–6 km. There, IASI/2 has nearly no bias, on average, at AM overpass. Note that the bias can be significant over specific scenarios or over selected subregions (see Sects. 4.2–4.3). The significant bias in the upper troposphere for IASI, about 11 % on average in the interval 7–12 km, is reduced to about the 5–6 % by IASI/2, which brings an improvement of more than 50 %.

We have also compared IASI and IASI/2 surface–6 km TOC pseudo-observations. IASI has RMSE, bias and Pearson coefficient of about 15.5 %, −2.5 % and 0.65. IASI/2 is able to retrieve the surface–6 km TOC with a 9 % RMSE, a −1 % bias and a 0.88 correlation coefficient (AM overpass); this is the 41 %, 54 % and 33 % better than for IASI. Results are only slightly worse for the PM overpass.

4.2 Tropospheric ozone distribution at regional scale

Here we present our analyses of the performances of IASI and IASI/2 to describe tropospheric ozone plumes at regional scale over Europe. We studied both spatial distributions and temporal evolutions.

Figure 7 shows the maps of the average surface–6 km TOC for August 2009, from raw and **AK**-smoothed MOCAGE pseudo-reality, and IASI and IASI/2 pseudo-observations. The differences of IASI and IASI/2 pseudo-observations with respect to raw MOCAGE pseudo-reality are also shown (bottom of the figure). In addition, Table 2 reports on the mean biases and RMSEs of IASI and IASI/2 pseudo-observations in the whole Europe and in four subregions: northern (latitude greater than 52.5° N)-land, northern-sea, southern (latitude smaller than 52.5° N)-land and southern-sea pixels. These results show that both IASI and IASI/2 underestimate the pseudo-reality at the southern subregion and overestimate it at the northern subregion. This effect is likely due to the small sensitivity of both pseudo-observations at the lowest levels (surface to 3 km). There, the a priori information prevails in the retrieval. Indeed, at southern locations high tropopauses are more likely, thus we use quite systematically the tropical a priori which is negatively biased with respect to MOCAGE pseudo-reality (see Fig. 5). The negative bias at southern locations is more marked over sea than over land. It should be mentioned that smaller thermal contrasts are expected over sea than over land. At northern locations, in particular at the north-west quadrant, we find a small overestimation. Also the overestimation is due to the scarce sensitivity at the lowest levels and to the effect of the low tropopause/mid-latitude a priori, which indeed tends to slightly overestimate the pseudo-reality (see Fig. 5). The areas of under-/overestimation are much less extended for IASI/2, and deviations are smaller. On average, IASI underestimates of over 10 % at the southern subregion (about 8 % over land and 12.5 % over sea), while IASI/2 underestimation is nearly 4.5 % over this region (about 3 % over land and 5.5 % over sea). IASI/2 may, therefore, reduce the systematic bias of IASI at southern Europe by more than 50 %. Overestimations at northern subregions are of the same magnitude for the two instruments, and generally small. No clear land/sea difference is found in the performances of IASI and IASI/2 at northern subregions. As for the RMSE, the values over the whole Europe are about 13.5 % for IASI and about 9.7 % for IASI/2. These values may be considered as a posteriori total errors and then compared to the theoretical errors on the surface–6 km TOC discussed in Sect. 3.1: only a very small overestimation of the a posteriori error is made by the theoretical total error calculation (0.1 and 0.2 DU overestimation for IASI and IASI/2, respectively), showing the coherence of our error estimations.

After the general characterization of pseudo-observations over Europe, we got some insights into the temporal evolution at continental to regional scale. To this aim, we study a

Table 1. Mean biases, RMSEs and Pearson coefficents, with respect to MOCAGE pseudo-reality, averaged over the altitude intervals 0–3 km, 0–6 km, 0–12 km and 7–12 km, for IASI and IASI/2 pseudo-observations for the AM and PM overpasses. Percent values of biases and RMSEs are reported in parentheses.

		0–3 km		0–6 km		0–12 km		7–12 km	
		IASI	IASI/2	IASI	IASI/2	IASI	IASI/2	IASI	IASI/2
AM	Bias [ppb]	−1.48 (−3.18 %)	−0.59 (−1.27 %)	−0.84 (−1.66 %)	−0.03 (−0.052 %)	2.96 (4.32 %)	1.77 (2.58 %)	10.13 (11.29 %)	5.04 (5.65 %)
	RMSE [ppb]	13.31 (28.48 %)	10.78 (23.17 %)	12.11 (23.90 %)	8.94 (17.61 %)	18.18 (26.54 %)	12.51 (18.29 %)	26.39 (29.63 %)	17.02 (19.08 %)
	Correlation	0.36	0.63	0.43	0.72	0.48	0.75	0.53	0.78
PM	Bias[ppb]	−3.50 (−7.31 %)	−2.71 (−5.67 %)	−2.22 (−4.33 %)	−1.49 (−2.89 %)	1.82 (2.62 %)	0.78 (1.12 %)	9.71 (10.73 %)	5.24 (5.80 %)
	RMSE [ppb]	15.70 (32.87 %)	12.92 (26.90 %)	14.58 (28.35 %)	10.76 (20.97 %)	22.91 (33.00 %)	14.88 (21.45 %)	34.84 (38.43 %)	19.94 (22.02 %)
	Correlation	0.24	0.56	0.30	0.65	0.35	0.71	0.41	0.78

Table 2. Mean biases and RMSEs for IASI and IASI/2 surface–6 km TOC pseudo-observations with respect to raw MOCAGE pseudo-reality, calculated in the whole Europe, north-land pixels, north-sea pixels, south-land pixels and south-sea pixels. The north/south limit latitude is 52.5° N. Percent values are reported in parentheses.

	Bias [DU(%)]		RMSE [DU(%)]	
	IASI	IASI/2	IASI	IASI/2
Europe	−0.99 (−4.66 %)	−0.43 (−1.77 %)	2.39 (13.51 %)	1.85 (9.67 %)
North-land	+0.31 (+2.38 %)	+0.21 (+2.17 %)	1.91 (10.89 %)	1.71 (8.26 %)
North-sea	+0.28 (+2.54 %)	+0.15 (+1.60 %)	1.99 (11.43 %)	1.77 (8.75 %)
South-land	−1.91 (−8.08 %)	−0.79 (−3.11 %)	2.40 (14.47 %)	1.89 (10.30 %)
South-sea	−2.68 (−12.40 %)	−1.46 (−5.42 %)	2.68 (16.01 %)	1.97 (11.01 %)

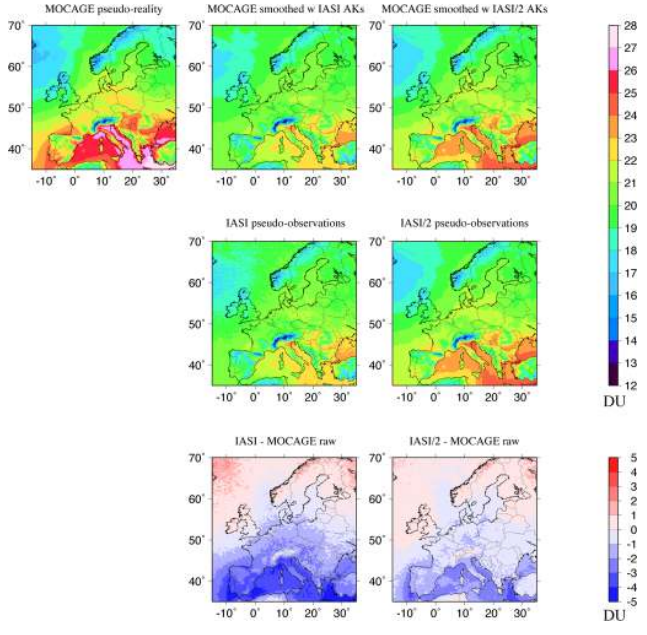

Fig. 7. Average surface–6 km TOC for August 2009, raw and **AK**-smoothed MOCAGE pseudo-reality (top), IASI and IASI/2 pseudo-observations (middle), differences (bottom) of IASI and IASI/2 pseudo-observations with respect to raw MOCAGE pseudo-reality.

peculiar LT ozone plume evolution occurring in the period 19–21 August 2009 and analyse how the two instruments are able to characterize this kind of phenomenon. These days are characterized by a pollution event. Figures 8 and 9 show the surface–6 km TOC from MOCAGE pseudo-reality, and IASI and IASI/2 pseudo-observations, for the 3 days. High values of the surface–6 km TOC over the South of France on the 19 August were moving toward the north-east, reaching the North of France to the Netherlands on the 20 August, and then Germany, Poland and the Scandinavian Peninsula on the 21 August (see first column of Figs. 8 and 9). In addition to this ozone plume evolution, some persistent high ozone levels can be seen over the Po Valley and the Mediterranean Basin. IASI/2 is able to better depict the ozone plume and its evolution, both for the AM and the PM overpasses. PM observations carry less information than AM observations, due to the smaller thermal contrasts during the PM overpass. In spite of this, PM observations by IASI/2 still contribute to the description of the ozone plume evolution, owing to the better performances of IASI/2 in presence of small sensitivity scenarios. Also the region with very small TOCs at the north-west quadrant and the area with very high values west of Galicia and Portugal on the 21 August are better identified by IASI/2. In general very high values of the surface–6 km TOC are not completely resolved by both instruments, especially when over the sea. In any case, IASI/2 appears to be able to better resolve the general patterns.

In order to analyse smaller regions showing a high ozone load, we focused our attention on some regional domains. Time series of raw MOCAGE surface–6 km TOC pseudo-reality, and IASI and IASI/2 pseudo-observations over Po Valley, eastern and western section of the Mediterranean Basin are shown in Fig. 10. The general feature over these regions, where we mainly used the high tropopause/tropical a

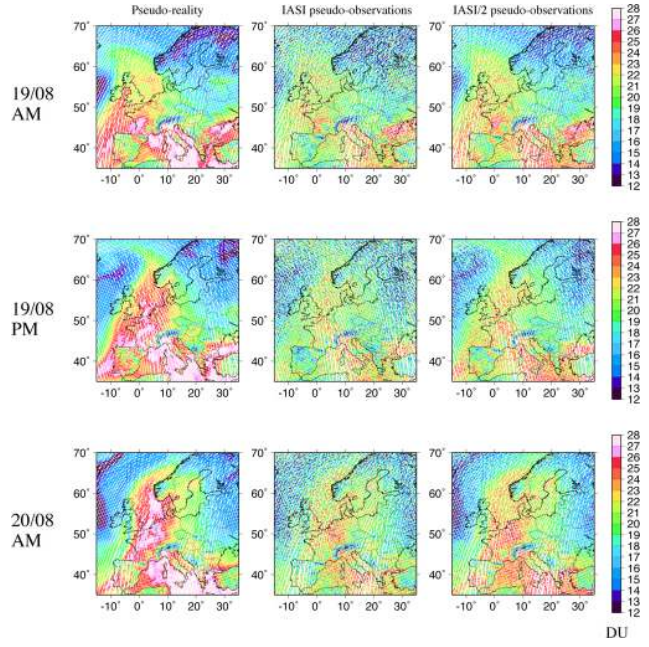

Fig. 8. Surface–6 km TOC for 19 August 2009 AM–20 August 2009 AM, MOCAGE pseudo-reality (column 1), IASI and IASI/2 pseudo-observations (columns 2 and 3).

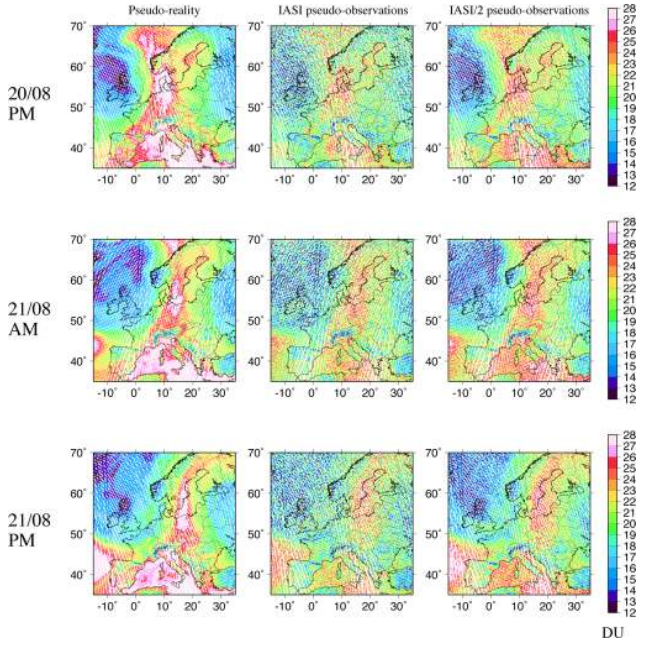

Fig. 9. Same as Fig. 8 but for 20 August 2009 PM–21 August 2009 PM.

priori, is a quite systematic underestimation of both pseudo-observations. The bias for IASI at these locations is in the range 10.5–13.5 %, while IASI/2 reduces biases of 50 to 60 %, reaching values as low as 4.0–6.0 %. A further systematic underestimation for PM overpasses is present, creating unrealistic oscillations (alternating day/night) in the time series. This latter effect is likely due to the smaller sensitivity at lower altitudes for the PM overpass, which is typically characterized by smaller thermal contrasts. This effect is strongly mitigated by IASI/2, see, e.g. the very strong oscillations in the IASI data set from 15 to 20 August over the Po Valley (Fig. 10a) and from 25 to 31 September over the western Mediterranean Region (Fig. 10c). As for the RMSEs and Pearson coefficients, IASI exhibits values in the range 11.0–14.5 % and 0.68–0.73, while IASI/2 can reach values as low as 4.5 % for the RMSE and 0.93 for the Pearson coefficient, at the western Mediterranean Region. Finally, the time series from IASI/2 follow quite well the temporal variability of MOCAGE pseudo-observations at regional scale, thus indicating that IASI/2 is better suitable than IASI for monitoring LT ozone at this spatial scale.

4.3 Local scale and air quality

In the present section, we investigate the behaviour of the two pseudo-observation data sets at a smaller spatial scale. We focus our analysis on some selected locations. The typical dimension of the areas is about $0.5° \times 0.5°$. The scope of these analyses is to evaluate the performances of IASI/2 for the monitoring of local evolutions of the LT ozone.

Time series of MOCAGE pseudo-reality, and IASI and IASI/2 pseudo-observations over Amsterdam, the Netherlands; Berlin, Germany; Paris, France; Barcelona, Spain; a marine location West of Norway's coasts (58.0° N–5.0° E) are shown in Fig. 11. We have selected these locations to have examples of urban scenarios at the northern part of Europe, at the southern part of Europe and a remote (marine) location. We aimed at evaluating the potential of IASI/2 over a set of different situations. We first discuss the urban locations in the northern part of Europe, those in Figs. 11a, b and c. For those pseudo-observations, the low tropopause/mid-latitude a priori is used for the majority of the retrievals, so no systematic negative biases are expected. As it is possible to see in Fig. 11, IASI/2, despite showing some slight underestimation, has proved to be significantly more sensitive to ozone peaks developing over short time periods (a few days) over northern European urban locations. To verify this sensitivity over evolution of a few days, refer to, for example, 24 August at Paris (Fig. 11c), 20–31 August at Amsterdam (Fig. 11a), 25 August at Berlin (Fig. 11b). More marked underestimations are observed over southern European urban locations, see the example of Barcelona in Fig. 11d. A systematic underestimation, due to the a priori, is expected over southern Europe, following from the results in Sect. 4.2. There, IASI/2 can significantly reduce the characteristic negative bias (about 45 % reduction of the negative bias at Barcelona, reaching a value of −7.7 %). Finally, as an example of remote locations we show a marine location over

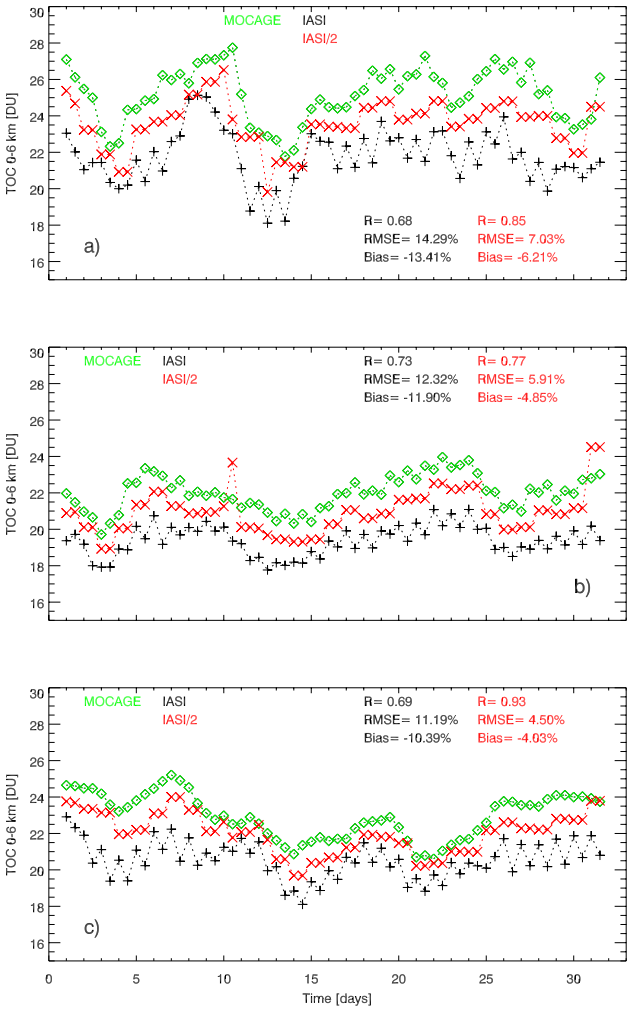

Fig. 10. Time series of MOCAGE pseudo-reality (green), and IASI (black) and IASI/2 pseudo-observations (red) over Po Valley **(a)**, eastern **(b)** and western section of the Mediterranean Basin **(c)**. Mean percent biases, percent RMSEs and Pearson coefficients are also reported for the two instruments.

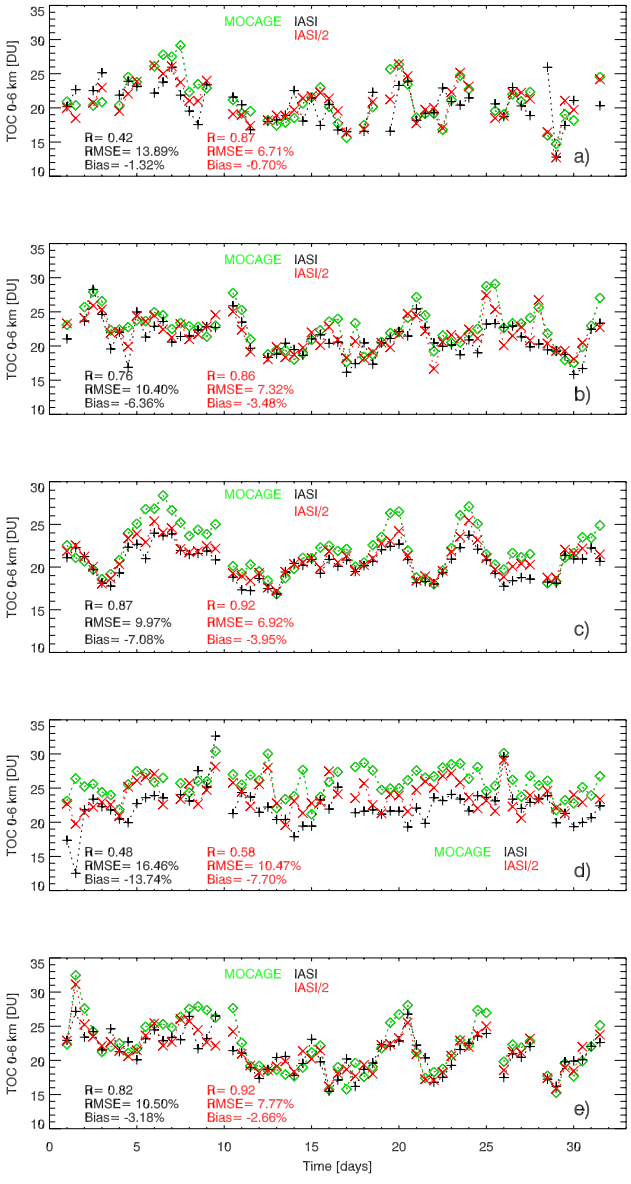

Fig. 11. Time series of MOCAGE pseudo-reality (green), and IASI (black) and IASI/2 pseudo-observations (red) over Amsterdam, the Netherlands **(a)**; Berlin, Germany **(b)**; Paris, France **(c)**; Barcelona, Spain **(d)**; a marine location West of Norway, 58.0° N–5° E **(e)**. Mean percent biases, percent RMSEs and Pearson coefficients are also reported for the two instruments.

the North Sea in Fig. 11e. There, both IASI and IASI/2 work pretty well, while IASI/2 still captures better the peaks probably related to small-scale transport phenomena, see, e.g. the case of 2 August.

As a complement to Fig. 11, MOCAGE pseudo-reality, IASI and IASI/2 pseudo-observations and a priori tropospheric profiles for the peak of the 24 August, AM overpass, in Paris, are shown in Fig. 12. The AKs from surface to 12 km, for IASI and IASI/2, for the same observation scenario, are also shown. In addition, maps of raw MOCAGE pseudo-reality and IASI and IASI/2 pseudo-observations for the days 25 and 11 August 2009 AM overpasses, and tropospheric ozone concentration profiles from a priori, MOCAGE pseudo-reality, and IASI and IASI/2 pseudo-observations over Berlin for the two days are reported in Fig. 13. The added value of IASI/2 may be related to a better sensitivity in the range 2–6 km, while marked peaks of the pseudo-reality from surface to 2 km are not generally detected. In any case, there still is a better sensitivity for IASI/2, see, e.g. 25 August at Berlin (Fig. 13). Vertical features of less than 2–3 km resolution are not caught by IASI/2, while features of about 4–5 km are sometimes caught by IASI/2 but not by IASI, whose typical vertical resolution is about 6–8 km (Boynard et al., 2009). The example of the retrieval

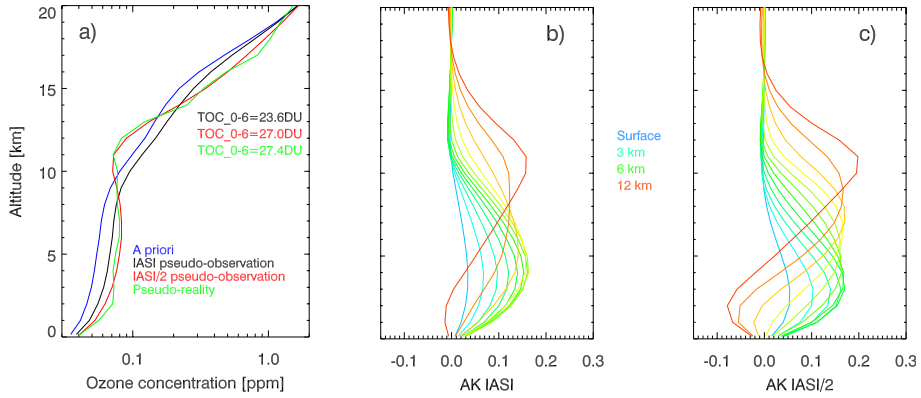

Fig. 12. MOCAGE pseudo-reality (green), IASI (black) and IASI/2 pseudo-observations (red) and a priori tropospheric profiles (blue) for the ozone peak of the 24 August in Paris (**a**); AKs from surface (sky blue) to 12 km (red) for IASI and IASI/2 (**b**, **c**) for the same scenario

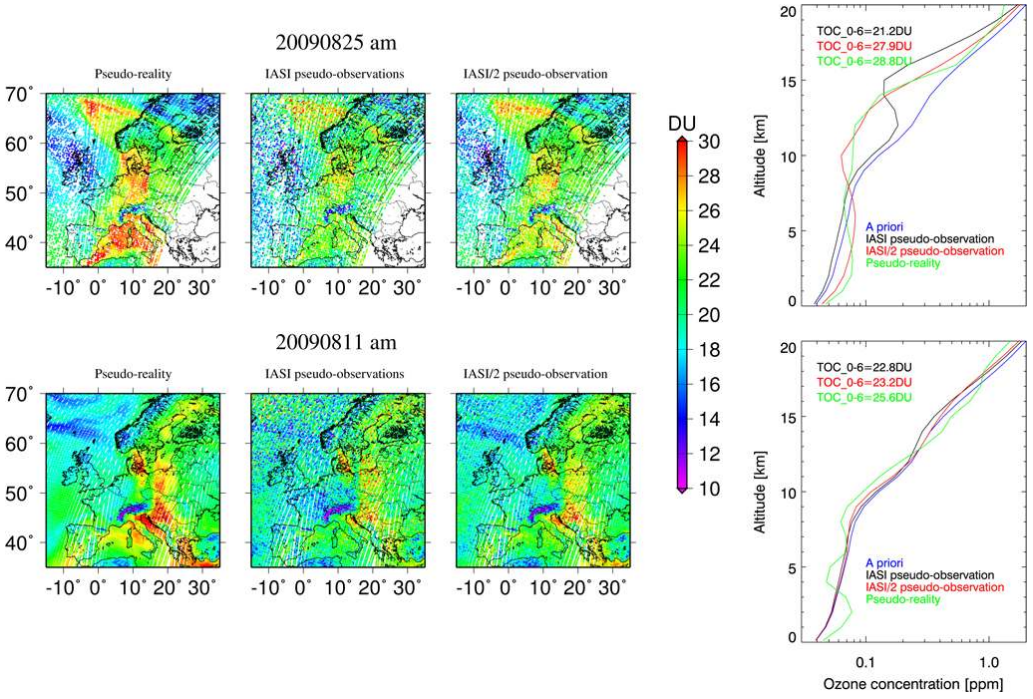

Fig. 13. Maps of raw MOCAGE pseudo-reality, and IASI and IASI/2 pseudo-observations for the days 25 (top) and 11 August 2009 (bottom), AM overpass. Vertical ozone concentration profiles from a priori (blue), MOCAGE pseudo-reality (green), and IASI (black) and IASI/2 pseudo-observations (red) over Berlin for the two days are also shown.

over Paris in Fig. 12 shows pretty well this latter aspect. The IASI pseudo-observation completely fails in retrieving the vertical behaviour of the pseudo-reality, which is characterized by a 4–5 km resolution oscillation at 9–13 km. While the IASI pseudo-observation is only shifted with respect to the a priori, IASI/2 was able to follow the vertical trend and, correspondingly, to detect also the enhanced values at the lowest layers. IASI/2 AKs show more sensitivity at 9 km, as well as at the mentioned interval 2–6 km (Fig. 12c). The AKs of the ranges 8–10 km are more peaked at the nominal altitudes, while for IASI they peak at higher or lower altitudes and values vanish at 7–9 km (Fig. 12b). A similar situation is shown in Fig. 13, for the 25 August over Berlin. The two retrievals are likely associated with the same plume, passing over the two cities in two consecutive days. For these two cases, the 24 August over Paris and the 25 August over Berlin, the surface–6 km TOC is markedly underestimated by IASI, while it is better estimated by IASI/2. On the contrary, the case of the 11 August over Berlin shows a typical situation where vertical features of about 2–3 km are not correctly retrieved by both IASI and IASI/2. The relatively high values of the surface–6 km TOC at Berlin on the 11 August can be

linked to a very localized pollution event, as it is possible to argue by seeing Fig. 13.

In general, our results suggest that IASI/2 is able to give, in several different situations, a significant added value with respect to IASI also for the monitoring of LT ozone at local scale, both at urban and remote locations. Sometimes, on the contrary, IASI/2 is not sufficiently sensitive, see, e.g. the entire time series of Barcelona or the case of Berlin, 11 August 2009.

5 Conclusions

We have presented a study of the performances of a possible configuration of IASI-NG (IASI-NG/IRS2, here called IASI/2) TIR nadir satellite instrument, based on a set of pseudo-observations generated by means of a new modular pseudo-observation simulator. IASI/2 pseudo-observations are compared with coincident IASI pseudo-observations. Here we want to stress how the scope of this study is not limited to the evaluation of the IASI-NG mission. Our results are of a general interest for the evaluation of the expected impact of next generation TIR LEO instruments observing the atmosphere with a nadir geometry. Our simulator is built with the KOPRA RTM and an embedded inversion algorithm routinely used to retrieve high quality lower tropospheric ozone information from the IASI real measurements. We have used the MOCAGE CTM to produce the pseudo-reality. We focused our attention on the LT ozone pseudo-observations to investigate how IASI/2 would impact the monitoring of ozone at spatiotemporal scales relevant to AQ. We based our analysis on one month, August 2009, AM and PM overpasses, of IASI and IASI/2 pseudo-observations. We found that IASI/2 brings a specific added value in the observation of local and short term ozone pollution phenomena and evolution of LT ozone plumes. This is due to the better vertical resolution in the troposphere resulting from better IASI/2 spectral resolution and noise. Our results suggest that IASI/2 is able to catch ozone vertical patterns of 4–5 km resolution while IASI has 6–8 km as the upper limit for the vertical resolution in the troposphere. This higher vertical resolution brings values as high as 0.70 DOFs for the surface–6 km TOC, with a maximum sensitivity at nearly 3.0 km altitude, which is about 30 % better, for the DOF, and more than 0.5 km lower, for the maximum sensitivity, than IASI. This allows an efficient separation of the lower from upper troposphere information also over low sensitivity scenarios, e.g. with a small or negative thermal contrast. In addition, the errors of the surface–6 km TOC, both from a priori theoretical and from a posteriori calculations, are reduced from the values of 2.5–2.4 DU (14.0–13.5 %), for IASI, to 2.0–1.8 DU (10.7–9.7 %), for IASI/2. According to our analysis, IASI/2 is expected to be able to very effectively reduce the marked underestimations that our inversion scheme shows over the southern European subregion, especially over sea pixels. The reduction of the bias can be more than 50 %. IASI/2 has been found more accurate in resolving and following ozone plume evolutions at continental scale, like the one observed in our pseudo-reality surface–6 km TOC for the period 19–21 August 2009, moving northwards and eastwards from South of France to the Scandinavian Peninsula. The most interesting result of our work is the improved capability of IASI/2 in monitoring small scale and short term pollution evolutions, therefore in a time–space scale more relevant for AQ. In particular, IASI/2 is found to be very effective in depicting LT ozone peak evolutions within time frames of a few days over urban locations. Scenarios of this kind have been selected, e.g. in Paris and Berlin urban areas, where IASI/2 has demonstrated its added value with respect to IASI. By the way, we found that vertical features with a resolution of 2–3 km are not well discriminated by IASI/2, nor very local ozone enhancements at the lowest altitude layers. All these results show how IASI/2 is a clear step forward towards a more effective monitoring of LT ozone at scales relevant for AQ from a low Earth orbit. Finally, we want to mention that the LT ozone variability at timescales shorter than 1 day gives a further constraint on the revisiting time and properly designed constellation of LEO instruments or, conversely, a geostationary observing system would be necessary for this issue.

Acknowledgements. The authors are grateful to CNRS-INSU for publication support. This work is carried on in the framework of the CNES/TOSCA/GeoQAir (quantification de l'apport d'une plateforme d'observations GÉOstationnaires pour la surveillance de la Qualité de l'AIR) and CNES/TOSCA/IASI-NG projects. We wish to thank the Institut für Meteorologie und Klimaforschung (IMK), Karlsruhe Institute of Technology (KIT), Germany, for a licence to use KOPRA radiative transfer model. The authors acknowledge the use of resources provided by the European Grid Infrastructure. For more information, please reference the EGI-InSPIRE paper (http://go.egi.eu/pdnon). MOCAGE data have been provided by Météo France. We wish to thank the two anonymous reviewers for their constructive criticism.

Edited by: M. Weber

The publication of this article is financed by CNRS-INSU.

References

Amann, M., Bertok, I., Cofala, J., Gyarfas, F., Heyes, C., Klimont, Z., Schöpp, W., and Winiwarter, W.: Baseline scenarios for the Clean Air For Europe (CAFE) programme, Tech. rep., International Institute for Applied Systems Analysis, for the European Commission Directorate General for Environment, Directorate C: Environment and Health, 2005.

Boynard, A., Clerbaux, C., Coheur, P.-F., Hurtmans, D., Turquety, S., George, M., Hadji-Lazaro, J., Keim, C., and Meyer-Arnek, J.: Measurements of total and tropospheric ozone from IASI: comparison with correlative satellite, ground-based and ozonesonde observations, Atmos. Chem. Phys., 9, 6255–6271, doi:10.5194/acp-9-6255-2009, 2009.

Clerbaux, C. and Crevoisier, C.: New Directions: Infrared remote sensing of the troposphere from satellite: Less, but better, Atmos. Environ., online first, doi:10.1016/j.atmosenv.2013.01.057, 2013.

Clerbaux, C., Boynard, A., Clarisse, L., George, M., Hadji-Lazaro, J., Herbin, H., Hurtmans, D., Pommier, M., Razavi, A., Turquety, S., Wespes, C., and Coheur, P.-F.: Monitoring of atmospheric composition using the thermal infrared IASI/MetOp sounder, Atmos. Chem. Phys., 9, 6041–6054, doi:10.5194/acp-9-6041-2009, 2009.

Crevoisier, C., Armante, R., Capelle, V., Chédin, A., Jacquinet-Husson, N., Scott, N., Stubenrauch, C., Clerbaux, C., George, M., Hadji-Lazaro, J., Payan, S., Guidard, V., Fourrié, N., Barret, B., Le Flochmoën, E., Dufour, G., Beekmann, M., Dauphin, P., Eremenko, M., Forêt, G., Sellitto, P., Herbin, H., Dubuisson, P., Parol, F., and Camy-Peyret, C.: Proposition de recherche scientifique spatiale: IASI-NG: coordination des activités de préparation de la mission IASI-Nouvelle Génération pour l'étude du climat, de la chimie atmosphérique et de la prévision numérique du temps, Tech. rep., CNRS, Comité Terre solide, océan, surfaces continentales, atmosphére, 2012.

Crutzen, P. J. and Stoermer, E. F.: The Anthropocene, Global Change Newsletter, 41, 17–18, 2000.

Cuesta, J., Eremenko, M., Liu, X., Dufour, G., Cai, Z., Höpfner, M., von Clarmann, T., Sellitto, P., Foret, G., Gaubert, B., Beekmann, M., Orphal, J., Chance, K., Spurr, R., and Flaud, J.-M.: Satellite observation of lowermost tropospheric ozone by multispectral synergism of IASI thermal infrared and GOME-2 ultraviolet measurements, Atmos. Chem. Phys. Discuss., 13, 2955–2995, doi:10.5194/acpd-13-2955-2013, 2013.

Dufour, A., Amodei, M., Ancellet, G., and Peuch, V.-H.: Observed and modelled "chemical weather" during ESCOMPTE, Atmos. Res., 74, 161–89, doi:10.1016/j.atmosres.2004.04.013, 2005.

Dufour, G., Eremenko, M., Orphal, J., and Flaud, J.-M.: IASI observations of seasonal and day-to-day variations of tropospheric ozone over three highly populated areas of China: Beijing, Shanghai, and Hong Kong, Atmos. Chem. Phys., 10, 3787–3801, doi:10.5194/acp-10-3787-2010, 2010.

Dufour, G., Eremenko, M., Griesfeller, A., Barret, B., LeFlochmoën, E., Clerbaux, C., Hadji-Lazaro, J., Coheur, P.-F., and Hurtmans, D.: Validation of three different scientific ozone products retrieved from IASI spectra using ozonesondes, Atmos. Meas. Tech., 5, 611–630, doi:10.5194/amt-5-611-2012, 2012.

Eremenko, M., Dufour, G., Foret, G., Keim, C., Orphal, J., Beekmann, M., Bergametti, G., and Flaud, J.-M.: Tropospheric ozone distributions over Europe during the heat wave in July 2007 observed from infrared nadir spectra recorded by IASI, Geophys. Res. Lett., 35, L18805, doi:10.1029/2008GL034803, 2008.

Fishman, J. and Larsen, J. C.: Distribution of total ozone and stratospheric ozone in the tropics: Implications for the distribution of tropospheric ozone, J. Geophys. Res., 92, 6627–6634, 1987.

Fu, D., Worden, J. R., Liu, X., Kulawik, S. S., Bowman, K. W., and Natraj, V.: Characterization of ozone profiles derived from Aura TES and OMI Radiances, Atmos. Chem. Phys. Discuss., 12, 27589–27636, doi:10.5194/acpd-12-27589-2012, 2012.

Hoepfner, M., Blom, C. E., Echle, G., Glatthor, N., Hase, F., and Stiller, G.: Retrieval simulations for MIPAS-STR measurements, in: IRS 2000: Current Problems in Atmospheric Radiation; Proceedings of the International Radiation Symposium, DEEPAK Publ., Hampton, V., 2001.

Horowitz, L. W.: Past, present, and future concentrations of tropospheric ozone and aerosols: Methodology, ozone evaluation, and sensitivity to aerosol wet removal, J. Geophys. Res., 111, D22211, doi:10.1029/2005JD006937, 2006.

Kulawik, S. S., Osterman, G., Jones, D. B. A., and Bowman, K. W.: Calculation of altitude-dependent Tikhonov constraints for TES nadir retrievals, IEEE Transactions on Geosciences and Remote Sensing, 44, 1334–1342, 2006.

Landgraf, J. and Hasekamp, O. P.: Retrieval of tropospheric ozone: the synergistic use of thermal infrared emission and ultraviolet reflectivity measurements from space, J. Geophys. Res., 112, D08310, doi:10.1029/2006JD008097, 2007.

Lin, M., Fiore, A. M., Horowitz, L. W., Cooper, O. R., Naik, V., Holloway, J., Johnson, B. J., Middlebrook, A. M., Oltmans, S. J., Pollack, I. B., Ryerson, T. B., Warner, J. X., Wiedinmyer, C., Wilson, J., and Wyman, B.: Transport of Asian ozone pollution into surface air over the western United States in spring, J. Geophys. Res., 117, D00V07, doi:10.1029/2011JD016961, 2012.

Liu, X., Chance, K., Sioris, C. E., Spurr, R. J. D., Kurosu, T. P., Martin, R. V., and Newchurch, M. J.: Ozone profile and tropospheric ozone retrieval from Global Ozone Monitoring Experiment (GOME): Algorithm description and validation, J. Geophys. Res., 110, D20307, doi:10.1029/2005JD006240, 2005.

Liu, X., Bhartia, P. K., Chance, K., Spurr, R. J. D., and Kurosu, T. P.: Ozone profile retrievals from the Ozone Monitoring Instrument, Atmos. Chem. Phys., 10, 2521–2537, doi:10.5194/acp-10-2521-2010, 2010.

Martin, V. R.: Satellite remote sensing of surface air quality, Atmos. Environ., 42, 7823–7843, doi:10.1016/j.atmosenv.2008.07.018, 2008.

McPeters, R. D., Labow, G. J., and Logan, J. A.: Ozone climatological profiles for satellite retrieval algorithms, J. Geophys. Res., 112, D05308, doi:10.1029/2005JD006823, 2007.

Monks, P., Granier, C., Fuzzi, S., Stohl, A., Williams, M., Akimoto, H., Amann, M., Baklanov, A., Baltensperger, U., Bey, I., Blake, N., Blake, R., Carslaw, K., Cooper, O., Dentener, F., Fowler, D., Fragkou, E., Frost, G., Generoso, S., Ginoux, P., Grewe, V., Guenther, A., Hansson, H., Henne, S., Hjorth, J., Hofzumahaus, A., Huntrieser, H., Isaksen, I., Jenkin, M., Kaiser, J., Kanakidou, M., Klimont, Z., Kulmala, M., Laj, P., Lawrence, M., Lee, J., Liousse, C., Maione, M., McFiggans, G., Metzger, A., Mieville, A., Moussiopoulos, N., Orlando, J., O'Dowd, C., Palmer, P., Parrish, D., Petzold, A., Platt, U., Pöschl, U., Pêvót, A., Reeves, C., Reimann, S., Rudich, Y., Sellegri, K., Steinbrecher, R., Simp-

son, D., ten Brink, H., Theloke, J., van der Werf, G., Vautard, R., Vestreng, V., Vlachokostas, C., and von Glasow, R.: Atmospheric composition change – global and regional air quality, Atmos. Environ., 43, 5268–5350, doi:10.1016/j.atmosenv.2009.08.021, 2009.

Munro, R., Siddans, R., Reburn, W. J., and Kerridge, B. J.: Direct measurement of tropospheric ozone distributions from space, Nature, 392, 171–98, 1998.

Natraj, V., Liu, X., Kulawik, S., Chance, K., Chatfield, R., Edwards, D. P., Eldering, A., Francis, G., Kurosu, T., Pickering, K., Spurr, R., and Worden, H.: Multi-spectral sensitivity studies for the retrieval of tropospheric and lowermost tropospheric ozone from simulated clear-sky GEO-CAPE measurements, Atmos. Environ., 45, 7151–7165, doi:10.1016/j.atmosenv.2011.09.014, 2011.

Ran, L., Zhao, C. S., Geng, F. H., Tie, X., Tang, X., Peng, L., Zhou, G., Yu, Q., Xu, J., and Guenther, A.: Ozone photochemical production in urban Shanghai, China: analysis based on ground level observations, J. Geophys. Res., 114, D15301, doi:10.1029/2008JD010752, 2009.

Rodgers, C. D.: Characterization and Error Analysis of Profiles Retrieved from Remote Sounding Instruments, J. Geophys. Res., 95, 5587–5595, 1990.

Rodgers, C. D.: Inverse methods for atmospheric sounding: Theory and practice, World Scientific Publishing Company, London, UK, 2000.

Schär, C. and Jendritzky, G.: Climate change: Hot news from summer 2003, Nature, 432, 559–560, doi:10.1038/432559a, 2004.

Schoeberl, M. R., Ziemke, J. R., Bojkov, B., Livesey, N., Duncan, B., Strahan, S., Froidevaux, L., Kulawik, S., Bhartia, P. K., Chandra, S., Levelt, P. F., Witte, J. C., Thompson, A. M., Cuevas, E., Redondas, A., Tarasick, D. W., Davies, J., Bodeker, G., Hansen, G., Johnson, B. J., Oltmans, S. J., Vömel, H., Allaart, M., Kelder, H., Newchurch, M., Godin-Beekmann, S., Ancellet, G., Claude, H., Andersen, S. B., Kyrö, E., Parrondos, M., Yela, M., Zablocki, G., Moore, D., Dier, H., von der Gathen, P., Viatte, P., Stübi, R., Calpini, B., Skrivankova, P., Dorokhov, V., de Backer, H., Schmidlin, F. J., Coetzee, G., Fujiwara, M., Thouret, V., Posny, F., Morris, G., Merrill, J., Leong, C. P., Koenig-Langlo, G., and Joseph, E.: A trajectory-based estimate of the tropospheric ozone column using the residual method, J. Geophys. Res., 112, D24S49, doi:10.1029/2007JD008773, 2007.

Sellitto, P., Bojkov, B. R., Liu, X., Chance, K., and Del Frate, F.: Tropospheric ozone column retrieval at northern mid-latitudes from the Ozone Monitoring Instrument by means of a neural network algorithm, Atmos. Meas. Tech., 4, 2375–2388, doi:10.5194/amt-4-2375-2011, 2011.

Sellitto, P., Del Frate, F., Solimini, D., and Casadio, S.: Tropospheric ozone column retrieval from ESA-Envisat SCIAMACHY nadir UV/VIS radiance measurements by means of a neural network algorithm, IEEE T. Geosci. Remote, 50, 998–1011, doi:10.1109/TGRS.2011.2163198, 2012a.

Sellitto, P., Di Noia, A., Del Frate, F., Burini, A., Casadio, S., and Solimini, D.: On the role of visible radiation in ozone profile retrieval from nadir UV/VIS satellite measurements: An experiment with neural network algorithms inverting SCIAMACHY data, J. Quant. Spectrosc. Ra., 113, 1429–1436, doi:10.1016/j.jqsrt.2012.04.007, 2012b.

Shindell, D. T., Faluvegi, G., Koch, D. M., Schmidt, G. A., Unger, N., and Bauer, S. E.: Improved Attribution of Climate Forcing to Emissions, Science, 326, 716–718, doi:10.1126/science.1174760, 2009.

Steck, T. and von Clarmann, T.: Constrained Profile Retrieval Applied to the Observation Mode of the Michelson Interferometer for Passive Atmospheric Sounding, Appl. Optics, 40, 3559–3571, 2000.

Stiller, G. P., von Clarmann, T., Funke, B., Glatthor, N., Hase, F., Höpfner, M., and Linden, A.: Sensitivity of trace gas abundances retrievals from infrared limb emission spectra to simplifying approximations in radiative transfer modelling, J. Quant. Spectrosc. Ra., 72, 249–280, doi:10.1016/S0022-4073(01)00123-6, 2002.

Vautard, R., Honore, C., Beekmann, M., and Rouil, L.: Simulation of ozone during the August 2003 heat wave and emission control scenarios, Atmos. Environ., 39, 3291–3303, 2005.

Wilson, R. C., Fleming, Z. L., Monks, P. S., Clain, G., Henne, S., Konovalov, I. B., Szopa, S., and Menut, L.: Have primary emission reduction measures reduced ozone across Europe? An analysis of European rural background ozone trends 1996–2005, Atmos. Chem. Phys., 12, 437–454, doi:10.5194/acp-12-437-2012, 2012.

WMO: Scientific assessment of ozone depletion: 2002, Executive Summary, Tech. Rep. 47, World Meteorological Organization, Geneva, Switzerland, 2002.

Worden, H. M., Logan, J. A., Worden, J. R., Beer, R., Bowman, K., Clough, S. A., Eldering, A., Fisher, B. M., Gunson, M. R., Herman, R. L., Kulawik, S. S., Lampel, M. C., Luo, M., Magretskaia, I. A., Osterman, G. B., and Shephard, M. W.: Comparisons of Tropospheric Emission Spectrometer (TES) ozone profiles to ozonesondes: Methods and initial results, J. Geophys. Res., 112, D03309, doi:10.1029/2006JD007258, 2007a.

Worden, J., Liu, X., Bowman, K., Chance, K., Beer, R., Eldering, A., Gunson, M., and Worden, H.: Improved tropospheric ozone profile retrievals using OMI and TES radiances, Geophys. Res. Lett., 34, L01809, doi:10.1029/2006GL027806, 2007b.

Ziemke, J. R., Chandra, S., and Bhartia, P. K.: Upper tropospheric ozone derived from the cloud slicing technique: Implications for large-scale convection, J. Geophys. Res., 108, 4390, doi:10.1029/2002JD002919, 2003.